

Hybrid Compressive Sampling via a New Total Variation TVL1^{*}

Xianbiao Shu and Narendra Ahuja

University of Illinois at Urbana-Champaign, Urbana, IL61801, USA,
`{xshu2, n-ahuja}@illinois.edu`

Abstract. Compressive sampling (CS) is aimed at acquiring a signal or image from data which is deemed insufficient by Nyquist/Shannon sampling theorem. Its main idea is to recover a signal from limited measurements by exploring the prior knowledge that the signal is sparse or compressible in some domain. In this paper, we propose a CS approach using a new total-variation measure TVL1, or equivalently TV_{ℓ_1} , which enforces the sparsity and the directional continuity in the gradient domain. Our TV_{ℓ_1} based CS is characterized by the following attributes. First, by minimizing the ℓ_1 -norm of partial gradients, it can achieve greater accuracy than the widely-used $\text{TV}_{\ell_1\ell_2}$ based CS. Second, it, named hybrid CS, combines low-resolution sampling (LRS) and random sampling (RS), which is motivated by our induction that these two sampling methods are complementary. Finally, our theoretical and experimental results demonstrate that our hybrid CS using TV_{ℓ_1} yields sharper and more accurate images.

1 Introduction

Digital images or signals are conventionally acquired by Nyquist/Shannon sampling. That requires, to incur no loss, the underlying analog signal must be sampled at Nyquist rate which is at least twice its highest analog frequency. The resulting raw digital data is too large to sense, transmit and store in many applications. One solution to this problem is the well-known image compression methodology, such as the JPEG2000 [20] compression standard, which represents a digital image by a smaller number of dominant components and relaxes the storage and transmission requirements. However, sensing a large image is still challenging.

Recently, compressive sensing [7] or particularly compressive sampling, has been introduced to address this problem more efficiently. CS exploits the redundancy present in the image at the time of sampling itself. Instead of sensing all the pixels that define the complete image, compressive sampling acquires a linear combination of randomly selected pixels and recovers the full image from these samples [16,17,3,22,8]. Instead of first sampling and then compressing, this imaging model avoids sampling of the redundant aspects of the data in the first place.

Compressive sampling assumes that an image, vectorized as \mathbf{I} of size L , can be represented as $\mathbf{I} = \Psi \mathbf{u}$ in some space, where \mathbf{u} has K non-zero elements (called K -sparsity). Instead of sensing \mathbf{u} directly in the Ψ domain, it may be easier to efficiently

^{*} The support of the National Science Foundation under grant IIS 08-12188 and the Office of Naval Research under grant N00014-09-1-0017 is gratefully acknowledged.

sample I in a different subspace defined by Φ . Then, sensing acquires a small number of projections of I onto this subspace such that $\mathbf{b} = \Phi\mathbf{I}$, where $\Phi \in \mathbb{C}^{M \times L}$ ($K < M < L$) is a sampling matrix. Given the measurements \mathbf{b} , CS recovers the K dominant components constituting \mathbf{u} . This translates into the problem of estimating the sparsest \mathbf{u} satisfying the measurement vector \mathbf{b} :

$$\min_{\mathbf{u}} \|\mathbf{u}\|_0 \quad \text{s. t.} \quad A\mathbf{u} = \Phi\Psi\mathbf{u} = \mathbf{b} \quad (1)$$

However, ℓ_0 -norm minimization is an NP-complete problem [15]. Fortunately, it has been proven that the intractable ℓ_0 -problem is equivalent to the convex minimization of $\|\mathbf{u}\|_1$, if the sampling matrix $A = \Phi\Psi$ obeys uniform uncertainty principle (UUP), introduced in [2] and refined in [4]. According to the definition in [4], a measurement matrix $A \in \mathbb{R}^{M \times L}$ is said to obey UUP with an oversampling factor λ , if the inequality

$$\frac{1}{2} \cdot \frac{M}{L} \|f\|_2^2 \leq \|Af\|_2^2 \leq \frac{3}{2} \cdot \frac{M}{L} \|f\|_2^2 \quad (2)$$

holds for all K -sparse signals f , where $K \leq M/(\alpha\lambda)$ and $\alpha > 0$ is a sufficiently large constant. According to [2], random sampling matrix and Fourier sampling matrix both obey UUP with $\lambda = \log(L/K)$ and $\lambda = \log^6(L/K)$ respectively. They are capable of recovering \mathbf{u} (with an overwhelming probability) from \mathbf{b} of size $M \geq \alpha K \log(L/K)$ and $M \geq \alpha K \log^6(L/K)$ respectively.

In addition to the sparsity in the Ψ -transform domain (wavelets [3,17], curvelets [10] et al.), compressive sampling often uses Total variation (TV) [18] to exploit the sparsity in finite difference domain. In some applications [10,13,12,24], Ψ -transform sparsity and TV are enforced together to improve the recovery accuracy as follows:

$$\min_{\mathbf{u}} \text{TV}(\Psi\mathbf{u}) + \beta \|\mathbf{u}\|_1 \quad \text{s. t.} \quad \|\Phi\Psi\mathbf{u} - \mathbf{b}\|_2^2 \leq \sigma^2 \quad (3)$$

Where β trades TV with Ψ -transform sparsity and σ^2 is the noise variance.

In this paper, we concentrate on how to evaluate and improve TV based compressive sampling. The most widely-used form of TV in CS [16,17,3,13,24] including Single-Pixel Camera (SPC) [8] is $\text{TV}_{\ell_1\ell_2}$, which computes the summation of the magnitudes of gradients (SMG) across the image: $\text{TV}_{\ell_1\ell_2}(\mathbf{I}) = \sum_i \sqrt{(D_h\mathbf{I})_i^2 + (D_v\mathbf{I})_i^2}$ where D_h and D_v are horizontal and vertical gradient operators. This TV measure has the following shortcomings: (1) The field of gradient magnitudes is not as sparse as partial gradients fields; (2) $\text{TV}_{\ell_1\ell_2}$ is prone to causing blurring across sharp edges, since SMG prefers to suppress large partial gradients; (3) SMG is a nonlinear operator, which makes it difficult to minimize $\text{TV}_{\ell_1\ell_2}$ efficiently. To seek a more efficient decoding algorithm, [14] uses an invertible operator Ω , which we call TV'_{ℓ_1} , given by $\Omega\mathbf{I} = \|D_h\mathbf{I}\|_1 + \|D_v\mathbf{I}\|_1$. However, TV'_{ℓ_1} seeks the intensity continuity horizontally and vertically, but fails to enforce the intensity continuity diagonally. Thus, to overcome these shortcomings of $\text{TV}_{\ell_1\ell_2}$ and TV'_{ℓ_1} , a new TV measure is needed.

In CS, random sampling is generally assumed to be near-optimal in reducing the sampled data for unstructured images [7,2]. [16,17,3] combine low-frequency sampling and random sampling, on intuitive grounds alone, without formal justification. In this paper, we present a hybrid CS method using a new TV measure with the following two contributions:

1. We propose a new TV measure TV_{ℓ_1} , which recovers piecewise smooth images with all possible sharp edges by exploiting the sparsity and continuity in the gradient domain. In addition, the UUP condition shows our TV_{ℓ_1} achieves higher accuracy and requires fewer measurements for the same quality of reconstruction than previous $\text{TV}_{\ell_1 \ell_2}$.
2. We present a theoretical analysis on hybrid sampling, which shows that low resolution sampling (LRS) and random sampling (RS) indeed complement each other for most natural images, and gives the criteria for the best combination of LRS and RS.

This paper is organized as follows. Section 2 describes our TV_{ℓ_1} based hybrid CS. Section 3 discusses implementation of our method. Section 4 presents experimental results. Section 5 gives concluding remarks.

2 Proposed TV Based Hybrid CS

Total variation $\text{TV}_{\ell_1 \ell_2}$ is a widely-used measure for enforcing intensity continuity and recovering a piecewise smooth image in CS [16,17,3,13,24]. In this paper, we propose a new TV measure TV_{ℓ_1} , which exploits the continuity and sparsity in the partial gradient domain. In comparison with $\text{TV}_{\ell_1 \ell_2}$, our TV_{ℓ_1} is able to recover sharper images with greater accuracy. Our TV_{ℓ_1} based CS problem can be formulated as follows.

$$\min_{\mathbf{I}} \text{TV}_{\ell_1}(\mathbf{I}) \quad \text{s. t.} \quad \Phi \mathbf{I} = \mathbf{b} \quad \text{and} \quad \Phi' \mathbf{I} = \mathbf{d} \quad (4)$$

where Φ is random sampling (RS) matrix or Fourier sampling matrix for large-scale images, and Φ' is low-resolution sampling (LRS) matrix, which acquires LR data d . To compare our TV_{ℓ_1} with $\text{TV}_{\ell_1 \ell_2}$ directly, we do not combine our TV_{ℓ_1} with any Ψ -transform sparsity, even if their combination might improve the recovery accuracy.

2.1 A New TV Measure

In this section, we present a new TV measure TV_{ℓ_1} . For intensity continuity in Fig. 1(a), the pixel $I_{i,j}$ is desired to be of similar value to its four neighbors in smooth regions.

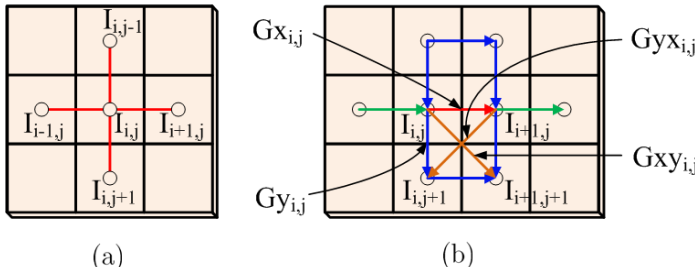


Fig. 1. (a) For intensity continuity, or gradient sparsity, we enforce each pixel, e.g. $I_{i,j}$, to be continuous with its 4 neighbors. (b) For gradient continuity, we enforce each partial gradient, e.g. $Gx_{i,j}$ marked as a red line, to be of similar value to its 6 neighbors marked as blue lines.

Similarly, partial gradients $Gx_{i,j} = I_{i+1,j} - I_{i,j}$ and $Gy_{i,j} = I_{i,j+1} - I_{i,j}$ can be continuous along all directions except their own directions, where they are desired to be discontinuous to obtain a sharp edge. Take $Gx_{i,j}$ (Fig. 1(b)) for example, our TV_{ℓ_1} will not enforce its continuity along the horizontal axis, but will do so along all other directions, as in Fig. 1(b)). For notational simplicity, we consider the continuity of partial gradients in a 2×2 neighborhood $(I_{i,j}, I_{i+1,j+1}, I_{i+1,j}, I_{i,j+1})$. The continuity constraints depend on the direction \vec{D} associated with the edge, if it exists in the neighborhood. For different cases of \vec{D} , the continuity constraints are:

$$\begin{cases} \|Gxx_{i,j}\|_1 = \|Gx_{i,j} - Gx_{i,j+1}\|_1 = 0 & \text{if } \vec{D} \text{ is vertical.} \\ \|Gyy_{i,j}\|_1 = \|Gy_{i,j} - Gy_{i+1,j}\|_1 = 0 & \text{if } \vec{D} \text{ is horizontal.} \\ \|Gxy_{i,j}\|_1 = \|Gx_{i,j} + Gy_{i+1,j}\|_1 = 0 & \text{if } \vec{D} \text{ is left-lower.} \\ \|Gyx_{i,j}\|_1 = \|Gy_{i,j} - Gx_{i,j}\|_1 = 0 & \text{if } \vec{D} \text{ is right-lower.} \end{cases}$$

Thus, we enforce the directional continuity of \mathbf{Gx} and \mathbf{Gy} by minimizing the ℓ_1 -norm of \mathbf{Gxy} , \mathbf{Gyx} , \mathbf{Gxx} and \mathbf{Gyy} . $Gxx_{i,j}$ is the derivative of $Gx_{i,j}$ along the vertical axis and $Gyy_{i,j}$ is the derivative of $Gy_{i,j}$ along the horizontal axis. Actually, $\|Gxx_{i,j}\|_1 = \|I_{i+1,j+1} + I_{i,j} - I_{i+1,j} - I_{i,j+1}\|_1 = \|Gyy_{i,j}\|_1$. By including the intensity continuity constraints in Fig. 1(a), we define our TV measure TV_{ℓ_1} as follows:

$$\text{TV}_{\ell_1}(\mathbf{I}) = \|\mathbf{Gx}\|_1 + \|\mathbf{Gy}\|_1 + \gamma(\|\mathbf{Gxy}\|_1 + \|\mathbf{Gyx}\|_1 + 2\|\mathbf{Gxx}\|_1) \quad (5)$$

where γ trades the intensity continuity with the gradient continuity. \mathbf{Gx} , \mathbf{Gy} , \mathbf{Gxy} and \mathbf{Gyx} are respectively horizontal, vertical, and two diagonal partial gradients in Fig. 1(b). Given our goal is to recover the sparsest gradients, $\|Gxx_{i,j}\|_1 = \|Gyy_{i,j}\|_1 = 0$ implies zero partial gradients along one of four directions in the 2×2 neighborhood, or equivalently $Gx_{i,j} = 0$, $Gy_{i,j} = 0$, $Gxy_{i,j} = 0$ or $Gyx_{i,j} = 0$. In this case, minimizing $\|\mathbf{Gxx}\|_1$ is redundant under the condition of minimal $\|\mathbf{Gx}\|_1 + \|\mathbf{Gy}\|_1 + \|\mathbf{Gxy}\|_1 + \|\mathbf{Gyx}\|_1$. Thus, our TV_{ℓ_1} can be simplified.

$$\text{TV}_{\ell_1}(I) = \|\mathbf{Gx}\|_1 + \|\mathbf{Gy}\|_1 + \gamma(\|\mathbf{Gxy}\|_1 + \|\mathbf{Gyx}\|_1) \quad (6)$$

This simplified TV_{ℓ_1} , enforces the sparsity and directional continuity in the gradient domain by seeking the γ -weighted sparsity of partial gradient fields $\mathbf{G} = [\mathbf{Gx}; \mathbf{Gy}; \mathbf{Gxy}; \mathbf{Gyx}]$.

In comparison with previous TV measures ($\text{TV}_{\ell_1\ell_2}$ and TV'_{ℓ_1}), our TV_{ℓ_1} based CS can recover any piecewise smooth image with all possible sharp edges (horizontal, vertical or diagonal), where the tuning parameter γ plays a crucial role in determining its preference. In general, TV-based CS seeks the image that has the minimal TV value and is closest to the measurements. The widely-used measure $\text{TV}_{\ell_1\ell_2}$ minimizes the sum of magnitudes of gradients (SMG) and penalizes larger partial gradients. Thus $\text{TV}_{\ell_1\ell_2}$ is prone to recovering a blurred image (Fig. 2(b)). TV'_{ℓ_1} , or equivalently a special case $\text{TV}_{\ell_1, \gamma=0}$, is prone to recovering an image of sharp horizontal and vertical edges in Fig. 2(c) by enforcing $\|\mathbf{Gx}\|_1 + \|\mathbf{Gy}\|_1$. However, these two images (Fig. 2(b)(c)) cause larger ℓ_1 -norm of \mathbf{Gxy} . $\text{TV}_{\ell_1, \gamma=1}$ equally penalizes the ℓ_1 -norm of each elements in the four partial gradient fields \mathbf{G} , whether large or small. So, $\text{TV}_{\ell_1, \gamma=1}$ is prone to recovering the sharp image of diagonal edges (Fig. 2(d)), since it has small $\text{TV}_{\ell_1, \gamma=1}$ and is closest to the original image (Fig. 2(a)).

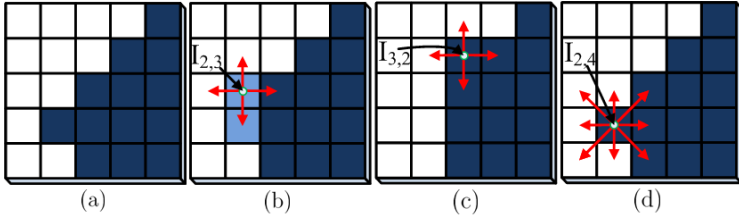


Fig. 2. Comparison of TV measures (the intensities of white, dark-blue and light-blue pixels are 1, 0 and 0.5). (a) Original sharp corner, (b) blurred image recovered by minimizing $\text{TV}_{\ell_1 \ell_2}$, (c) straight edge image recovered by minimizing $\text{TV}_{\ell'_1}$, (d) diagonal corner image recovered by minimizing $\text{TV}_{\ell_1, \gamma=1}$.

Table 1. The sparsity of a 256×256 LENA image in the field of gradient magnitudes and the four partial gradient fields. The partial gradient fields has similar sparsity, which is much smaller than that of the gradient magnitude field.

$\sqrt{\text{Gx}^2 + \text{Gy}^2}$	Gx	Gy	Gxy	Gyx
40652	28111	27767	28760	28633

2.2 UUP Condition for TV_{ℓ_1} Based CS

In this section, we present the UUP condition for TV based compressive sampling. According to this UUP condition, we compare our TV_{ℓ_1} and previous $\text{TV}_{\ell_1 \ell_2}$ in terms of the number of measurements for lossless recovery. An image \mathbf{I} can be represented as a linear combination of each partial gradient field plus some constant values, i.e., $\mathbf{I} = \Psi_x \mathbf{Gx} + \mathbf{Ix} = \Psi_y \mathbf{Gy} + \mathbf{Iy} = \Psi_{xy} \mathbf{Gxy} + \mathbf{Ixy} = \Psi_{yx} \mathbf{Gyx} + \mathbf{Iyx}$, where constant vectors \mathbf{Ix} , \mathbf{Iy} , \mathbf{Ixy} and \mathbf{Iyx} are equal to some rearrangements of the first row pixels as well as the first and last column pixels. For instance, \mathbf{Ix} is a repetition of the first column pixels. According to (4), $b = \Phi \mathbf{I} = \Phi \Psi_x \mathbf{Gx} + \Phi \mathbf{Ix} = \Phi \Psi_y \mathbf{Gy} + \Phi \mathbf{Iy} = \Phi \Psi_{xy} \mathbf{Gxy} + \Phi \mathbf{Ixy} = \Phi \Psi_{yx} \mathbf{Gyx} + \Phi \mathbf{Iyx}$. Suppose $\gamma = 1$ and no LRS for simplicity, our TV_{ℓ_1} based CS problem (4) is reformulated as:

$$\min_{\mathbf{G}} \|\mathbf{G}\|_1 \quad \text{s. t.} \quad A\mathbf{G} = [\mathbf{bx}; \mathbf{by}; \mathbf{bxy}; \mathbf{byx}] \quad (7)$$

where the partial gradient fields $\mathbf{G} = [\mathbf{G}_1; \mathbf{G}_2; \mathbf{G}_3; \mathbf{G}_4] = [\mathbf{Gx}; \mathbf{Gy}; \mathbf{Gxy}; \mathbf{Gyx}]$, the sampling matrix $A = \text{diag}(A_1, A_2, A_3, A_4) = \text{diag}(\Phi \Psi_x, \Phi \Psi_y, \Phi \Psi_{xy}, \Phi \Psi_{yx})$, and the sampled data $[\mathbf{bx}; \mathbf{by}; \mathbf{bxy}; \mathbf{byx}] = [\mathbf{b} - \Phi \mathbf{Ix}; \mathbf{b} - \Phi \mathbf{Iy}; \mathbf{b} - \Phi \mathbf{Ixy}; \mathbf{b} - \Phi \mathbf{Iyx}]$.

If replacing the objective function with $\sqrt{\mathbf{Gx}^2 + \mathbf{Gy}^2}$, we induce the $\text{TV}_{\ell_1 \ell_2}$ based CS problem. The major difference between these two TV is $\text{TV}_{\ell_1 \ell_2}$ enforces the sparsity in the gradient magnitude fields and TV_{ℓ_1} enforces that of partial gradients.

Now, we compare the sparsity (denote its maximal value as K_1) in each partial gradient field and that (denoted as K_2) in the gradient magnitude field. For most natural images, it is generally true that $K_1 \leq K_2$, as shown in Table 2. In the gradient magnitude field $\sqrt{\mathbf{Gx}^2 + \mathbf{Gy}^2}$, K_2 is equal to the size of pixels having non-zero

\mathbf{Gx} or \mathbf{Gy} . Thus, K_2 is larger than both the sparsity of \mathbf{Gx} and that of \mathbf{Gy} . At each pixel, the gradient magnitude is equal to $\sqrt{Gx_{i,j}^2 + Gy_{i,j}^2}$, the diagonal gradients $Gxy_{i,j} = Gx_{i,j} + Gy_{i+1,j}$ and $Gyx_{i,j} = Gy_{i,j} - Gx_{i,j}$. So, the sparsity of diagonal gradients \mathbf{Gxy} or \mathbf{Gyx} is smaller than K_2 , which equals the size of pixels having non-zero \mathbf{Gx} or \mathbf{Gy} . Thus, we prove that $K_1 \leq K_2$ for any image.

According to (7), each individual sampling matrix $A_i, i = 1, 2, 3, 4$, corresponds to a partial gradient field \mathbf{G}_i (size $N^2 \times 1$, image size: $N \times N$). For each random sampling matrix $A_i \in \mathbb{R}^{M \times N^2}, 1 \leq i \leq 4$ to obey the UUP condition (2), the inequality

$$\frac{1}{2} \cdot \frac{M}{N^2} \|\mathbf{G}_i\|_2^2 \leq \|A_i \mathbf{G}_i\|_2^2 \leq \frac{3}{2} \cdot \frac{M}{N^2} \|\mathbf{G}_i\|_2^2 \quad (8)$$

must hold for any partial gradient \mathbf{G}_i whose sparsity satisfies $K_1 \leq M/(\alpha \log(N^2/M))$. In other words, each $A_i \in \mathbb{R}^{M \times N^2}$ obeys the UUP condition, provided that $M \geq \alpha K_1 \log(N^2/K_1)$. In our TV_{ℓ_1} based CS (7), we need to induce the UUP condition of the big matrix A which involves all four gradient fields \mathbf{G} . By summing the 4 components in (8), we obtain the inequality for the matrix A :

$$\begin{aligned} \frac{1}{2} \cdot \frac{M}{N^2} \sum_i \|\mathbf{G}_i\|_2^2 &\leq \sum_i \|A_i \mathbf{G}_i\|_2^2 \leq \frac{3}{2} \cdot \frac{M}{N^2} \sum_i \|\mathbf{G}_i\|_2^2 \\ \frac{1}{2} \cdot \frac{M}{N^2} \|\mathbf{G}\|_2^2 &\leq \|A \mathbf{G}\|_2^2 \leq \frac{3}{2} \cdot \frac{M}{N^2} \|\mathbf{G}\|_2^2 \end{aligned} \quad (9)$$

Obviously, the combined sampling matrix A obeys the UUP condition, given that each sampling matrix $A_i, i = 1, 2, 3, 4$ obeys the UUP condition, or given the condition $M \geq \alpha K_1 \log(N^2/K_1)$. Suppose the gradient magnitude is sampled randomly, we can induce that the number of measurements required by previous $\text{TV}_{\ell_1 \ell_2}$ based CS is $M \geq \alpha K_2 \log(N^2/K_2)$.

Therefore, our TV_{ℓ_1} based compressive sampling requires fewer samples than $\text{TV}_{\ell_1 \ell_2}$ for the same quality of reconstruction. In other words, based on the same number of measurements, our TV_{ℓ_1} based CS will recover an image of higher quality.

2.3 Optimal Hybrid Sampling

For most natural images, our hybrid sampling (4) consisting of low-resolution sampling (LRS) and random sampling (RS) requires fewer measurements than random sampling alone for the same quality of reconstruction. In this section, we will give a theoretical analysis on the optimal hybrid sampling and its minimal number of measurements for lossless reconstruction.

Both low resolution sampling (LRS) and random sampling (RS) aim at reducing the size of sampled data non-adaptively. The major difference is that LRS measures the low-frequency information with averaging filter (block size: $n \times n$, frequency $F = 1/n$) while RS senses the combination of randomly-selected data.

To demonstrate how RS and LRS complement each other in our TV_{ℓ_1} based CS, we develop a hierarchical gradient transform (HGT), similar to Wavelet transform. HGT consists of an average basis Ψ'' at the coarsest level and a series of difference bases

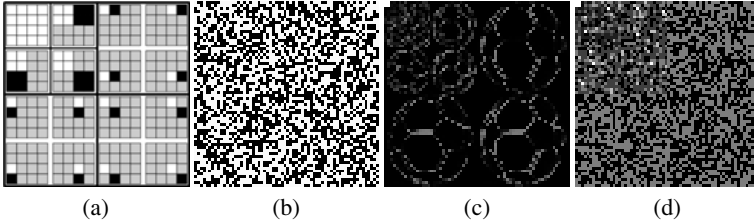


Fig. 3. (a) Hierarchical gradient transform (HGT), (b) a Bernoulli random matrix, magnitude of HGT of (c) a Ball image and (d) the Bernoulli random matrix

Ψ' at finer levels (Fig. 3(a)). Consider a 2×2 block at the finest level, all the partial gradients inside this block are highly correlated. Thus, our HGT represents these partial gradients by three partial gradients at the left-upper pixel. Similarly, we can de-correlate the partial gradients in larger scale 2×2 blocks at coarser levels, as shown in Fig. 3(a). Thus, given an image, HGT outputs a series of hierarchical gradients \mathbf{G}' and some average responses.

For a piecewise smooth image, \mathbf{G}' has denser non-zero elements at coarser levels (Fig. 3(c)) while Bernoulli random sampling (RS) senses \mathbf{G}' almost uniformly in the HGT domain (Fig. 3(d)). Thus, sole RS is not efficient and hybrid sampling is desired. In hybrid sampling (4), given LR samples \mathbf{d} at coarser levels, we measure \mathbf{G}' on the rest finer levels (denoted by \mathbf{G}'_d) by random sampling (RS). Since \mathbf{G}'_d is quite sparse, hybrid sampling sacrifices some low-resolution samples \mathbf{d} for dramatically reducing the number of RS measurements b.

An $N \times N$ image \mathbf{I} can be represented as linear combinations of LR samples \mathbf{d} on coarser scales and K'_d -sparsity \mathbf{G}'_d associated with \mathbf{d} , $\mathbf{I} = \Psi' \mathbf{G}'_d + \Psi'' \mathbf{d}$. For the sake of simplicity, we approximate our TV_{ℓ_1} minimization by enforcing the sparsest \mathbf{G}'_d , and reformulate (4) as follows:

$$\min_{\mathbf{G}'_d} \|\mathbf{G}'_d\|_1 \quad \text{s. t.} \quad A' \mathbf{G}'_d = \Phi \Psi' \mathbf{G}'_d = \mathbf{b} - \Phi \Psi'' \mathbf{d} \quad (10)$$

where A' is the sampling matrix. The minimal number of measurements for the lossless reconstruction is $\alpha K'_d \log(N^2 / K'_d)$, where α is a constant.

Proposition 1. *The hybrid sampling approach consisting low-resolution sampling ($F = 1/n$) and M random projections is capable of recovering the original image (size $N \times N$), if the sampling matrix A' obeys UUP [2] for the unknown K'_d -sparsity coefficients \mathbf{G}'_d at the finer levels of HGT. Consequently, for lossless reconstruction, the minimal number of measurements M_{\min} equals $(N/n)^2 + \alpha K'_d \log((N^2 - (N/n)^2)/K'_d)$, where α is a constant.*

The optimal hybrid sampling depends on selection of LRS, which is defined by its frequency ($F = 1/n$) and other parameters, such as d and K'_d . By varying LRS and its corresponding RS, we can seek the optimal hybrid sampling with the smallest number of measurements ($\hat{M}_{\min} = (N/\hat{n})^2 + \alpha \hat{K}'_d \log((N^2 - (N/\hat{n})^2)/\hat{K}'_d)$), where $1/\hat{n}$ is the frequency of the optimal LRS.

3 Implementation Issues

3.1 Practical Hybrid Sampling

One problem with random sampling is its inefficiency for large-scale images. The notable CS application of random sampling is Single Pixel Camera (SPC)[22,8], which is advantageous over the conventional pixel-array camera in reducing sampling rate (ratio of sample size and data size, denoted as R). It sequentially acquires random linear measurements of scene brightness by a digital micro-mirror (DMD) and thus its sensing rate is limited. To date, DMD can provide at most 32000 random patterns/second. Suppose we need to capture an image of size 1024×768 at $R = 10\%$, then the sensing process takes $1024 \times 768 \times 0.1/32000 = 2.46$ seconds. Our hybrid sampling can increase the frame rate (RS) by incorporating some LR samples and even reduce the total sampled data from RS and LR, for the same quality of reconstruction.

Another problem with random sampling is its high computational cost. For instance, to recover a 1024×768 image at $R = 10\%$, we need more than 7 gigabytes of memory just to store the Bernoulli random matrix. To reduce the cost of time and memory, many efforts have been made to develop structural sampling methods (Fourier transform[12], scrambled Fourier[1], Hadarmard transform[9], Noiselet[6,3]). A typical application of structural sampling is Magnetic Resonance Imaging (MRI)[12] using Fourier sampling.

3.2 Sparsity Decoding

In this section, we present our approach to recover the image from the limited measurements by decoding the sparse gradient \mathbf{G} . There is a number of algorithms available for decoding, including Orthogonal Matching Pursuit (OMP)[23], Basis Pursuit(BP)[5] listed in SparseLab Toolbox[21], second-order cone programming (SOCP) implemented in ℓ_1 -Magic[11], and iterative shrinkage/thresholding (IST)[24].

For decoding, we aim to solve (4) and recover the image \mathbf{I} and its sparse partial gradients \mathbf{G} . We employ a primal-dual interior-point optimization routine called PDCO [19]. Since random sampling is computationally costly, we need to replace it by Fourier sampling for sensing large-scale images. Given the partial Fourier data \mathbf{b} , we use the IST method [24] to solve (4) to recover the image \mathbf{I} .

4 Experimental Results

In this section, we present some experimental results to compare our hybrid compressive sampling using TV_{ℓ_1} , with the widely-used $\text{TV}_{\ell_1\ell_2}$ based CS method. We present results for both qualitative (visual) and quantitative evaluations.

4.1 Selection of Parameter γ

As shown in (6), our TV_{ℓ_1} seeks the γ -weighted gradient sparsity and recovers images with sharp edges. For a sharp image containing 40% diagonal edges, our TV_{ℓ_1} can achieve much higher accuracy than $\text{TV}_{\ell_1\ell_2}$ and its accuracy depends on selection of γ (Fig. 4(a)). As shown in Fig. 4(b), in comparison with other TV measure, our TV_{ℓ_1}

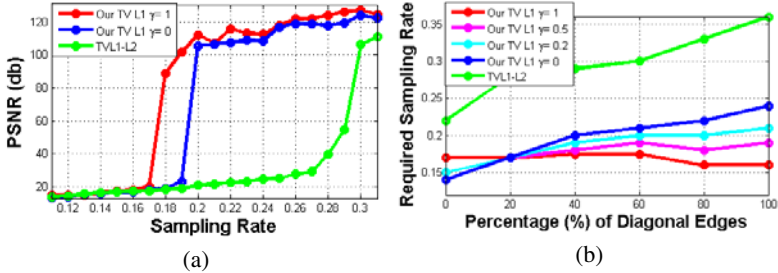


Fig. 4. Comparison of TV measures. (a) The recovery accuracy of a sharp image in which 40% of edges are diagonal. (b) The required sampling rates on different images, for the recovery accuracy (PSNR) to be large than 40dB.

($\gamma = 1$) requires fewer samples at images containing many diagonal edges and more samples at images containing few diagonal edges, for the same recovery accuracy. That means, the value of the optimal γ should be proportional to the percentage of diagonal edges in the image. This result is consistent with the claim that our TV_{ℓ_1} can recovery all possible sharper edges (vertical, horizontal or diagonal) in Sect. 2.1. In our following experiments, the optimal γ is selected as $0.2 \leq \gamma \leq 1$.

4.2 Hybrid Compressive Sampling via Our TV_{ℓ_1}

To show the advantage of our TV_{ℓ_1} over $\text{TV}_{\ell_1\ell_2}$, we choose small piecewise smooth images, e.g., ECCV image in Fig. 5 and Ball image in Fig. 6, due to the expensive sparsity decoding. As shown in Fig. 5, our TV_{ℓ_1} based CS is able to reconstruct the sharp ECCV image almost perfectly while $\text{TV}_{\ell_1\ell_2}$ causes serious artifacts at $R = 25\%$. Our TV_{ℓ_1} is still advantageous over previous $\text{TV}_{\ell_1\ell_2}$ at varying sampling rates (Fig. 5(c)). As shown in Fig. 6, Ball image is almost a real image, except that we remove some noise in the gray region. Given the same sampled data, our TV_{ℓ_1} acquires an image (Fig. 6(b)) whose Peak-Signal-Noise-Ratio (PSNR) is 3.0dB higher than that recovered by previous $\text{TV}_{\ell_1\ell_2}$ (Fig. 6(a)).

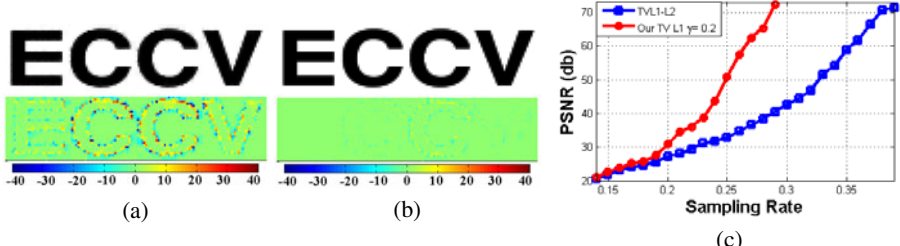


Fig. 5. Recovered ECCV images (upper) and error maps (lower) by (a) $\text{TV}_{\ell_1\ell_2}$ (PSNR=32.88dB) and (b) TV_{ℓ_1} (PSNR=48.17dB) at the sampling rate $R = 25\%$ (LRS:6.25% and RS:18.75%). (c) Comparison of TV measures on ECCV image sensed by our hybrid sampling with LRS ($F = 1/4$).

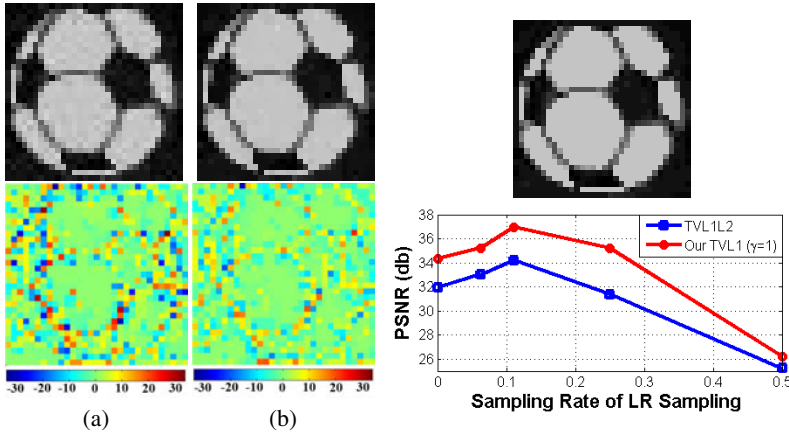


Fig. 6. Given random sampling (41%) and LR sampling ($F = 1/3$) on Ball image (upper-right), images recovered by (a) $\text{TV}_{\ell_1\ell_2}$ (PSNR=29.8dB) with its error map, and (b) TV_{ℓ_1} (PSNR=32.8dB) with its error map. Given the fixed total hybrid sampling rate ($R = 60\%$), we show the recovery accuracy of TV_{ℓ_1} and $\text{TV}_{\ell_1\ell_2}$ at varying LR sampling rates (lower-right).

Table 2. The estimated and real minimal number of required measurements on the Ball image ($N=32$), for each hybrid sampling methods associated with different LRS (block size: $n \times n$)

$n \times n$ LRS	K'_1	Esti. M_{min} at $\alpha = 1.2$	Real M_{min} for $\text{PSNR} \geq 40 \text{ dB}$
No LRS	576	$0 + 576\alpha = 691$	717
4×4	512	$64 + 512\alpha = 678$	680
3×3	440	$121 + 440\alpha = 649$	653
2×2	368	$256 + 368\alpha = 698$	665
2×1	250	$512 + 235\alpha = 794$	756

For most natural images, low-resolution sampling (LRS) and random sampling (RS) can complement each other. For instance, the recovery accuracy of our TV_{ℓ_1} is improved by combining RS with LRS ($F = 1/3$) on Ball image (Fig. 6). As shown in Fig. 6, both our TV_{ℓ_1} and previous $\text{TV}_{\ell_1\ell_2}$ achieve the optimal accuracy at the LRS ($F = 1/3$), given the total sampling rate $R = 60\%$.

According to Proposition 1, we can determine the optimal hybrid sampling that requires the fewest samples M_{min} . Now, we want to verify Proposition 1 by some experimental results. Since K'_1 is comparable to $N^2 - (N/n)^2$, we approximate the estimated M_{min} by $(N/n)^2 + \alpha K'_1$. Table 4.2 shows one successful case ($\alpha = 1.2$), in which our estimated M_{min} is close to the real M_{min} required to achieve the accuracy (PSNR = 40dB). At $\alpha = 1.2$, hybrid sampling with LRS ($F = 1/3$) requires the smallest M_{min} and thus is optimal, which is consistent with the accuracy chart in Fig. 6.

4.3 Evaluation of Our TV_{ℓ_1} by Fourier Sampling

Now, we evaluate our TV_{ℓ_1} based CS on two real MR images (Chest and Bone) by Fourier sampling ([12]). Given 14% Fourier samples, our TV_{ℓ_1} can recover a Chest image I_1 (Fig. 7(c)), whose PSNR is 1.3dB higher than that I_2 (Fig. 7(b)) by $TV_{\ell_1\ell_2}$. Figure 7(g) shows the difference map $I_d = I_1 - I_2$, which is close to the second derivatives of Chest image (Fig. 7(a)). Similarly, the region boundary (Fig. 7(f)) in Bone image recovered from our TV_{ℓ_1} is obviously sharper than that in Fig. 7(e), which is also demonstrated by their difference map (Fig. 7(h)). Thus, our TV_{ℓ_1} is prone to enforcing sparse partial gradients in piecewise smooth images. Besides, our TV_{ℓ_1} achieves higher accuracy at varying sampling rates than $TV_{\ell_1\ell_2}$ in recovering these images, as shown in Fig. 7(i).

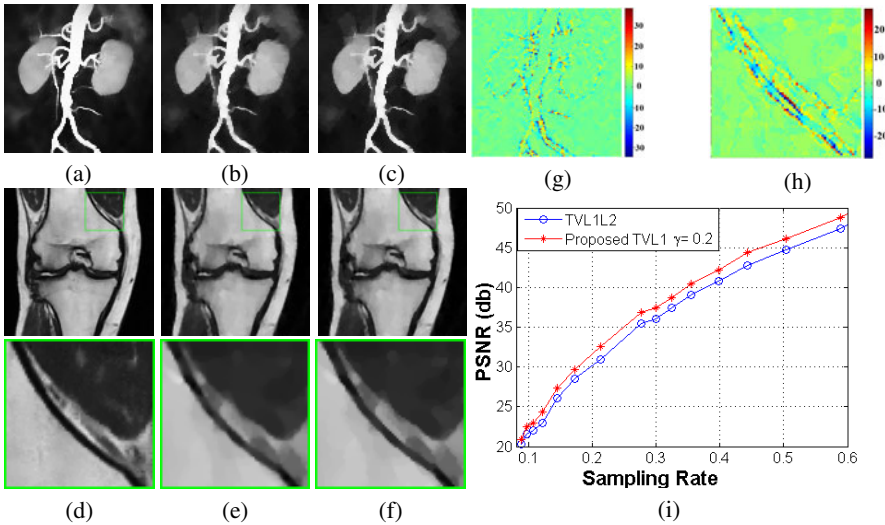


Fig.7. Comparison of TV measures by Fourier sampling. (a) Original Chest image sensed at $R = 14\%$, images recovered by (b) $TV_{\ell_1\ell_2}$ (PSNR= 26.0dB) and (c) TV_{ℓ_1} (PSNR=27.3dB). (d) Original Bone image sensed at $R = 9.34\%$, images recovered by (e) $TV_{\ell_1\ell_2}$ (PSNR=27.1dB) and (f) TV_{ℓ_1} (PSNR=27.6dB). (g) Difference of (c)and (b). (h) Difference of (f)and (e). (i) Accuracy vs. sampling rate on Chest image.

5 Conclusion

In this paper, we propose a hybrid compressive sampling method using a new TV measure TV_{ℓ_1} , for recovering a piecewise smooth image containing all possible sharper edges from limited measurements. We induce a UUP condition for TV based compressive sampling, which shows that our TV_{ℓ_1} requires fewer measurements than widely used $TV_{\ell_1\ell_2}$ for the same quality reconstruction. In addition, some theoretical analysis is presented to show the advantage of hybrid sampling over random sampling for most natural images and how to seek the optimal hybrid sampling. Finally, our TV_{ℓ_1} based hybrid CS achieves better performance in experimental results.

References

1. Candes, E., Romberg, J., Tao, T.: Stable signal recovery from incomplete and inaccurate measurements. *Comm. Pure Appl. Math.* 59(8), 1208–1223 (2006)
2. Candes, E., Tao, T.: Near-optimal signal recovery from random projections and universal encoding strategies? *IEEE Transactions on Information Theory* 52(12), 5406–5245 (2006)
3. Candes, E., Romberg, J.: Sparsity and incoherence in compressive sampling. *Inverse Prob.* 23(3), 969–986 (2007)
4. Candes, E., Tao, T.: Decoding by linear programming. *IEEE Transactions on Information Theory* 51, 4203–4215 (2005)
5. Chen, S., Donoho, D.: Atomic decomposition by basic pursuit. *SIAM J. Sci. Comp.* 20, 33–61 (1998)
6. Coifman, R., Geshwind, F., Meyer, Y.: Noiselets. *Appl. Comp. Harmonic Analysis* 10, 27–44 (2001)
7. Donoho, D.: Compressed sensing. *IEEE Trans. on Information Theory* (2006)
8. Duarte, M.F., Davenport, M.A., Takhar, D., et al.: Single-pixel imaging via compressive sampling. *IEEE Signal Processing Magazine* 25(2), 83–91 (2008)
9. Gan, L., Do, T., Tran, T.: Fast compressive imaging using scrambled block hadamard ensemble. *EUSIPCO*
10. He, L., Chang, T.C., Osher, S., Fang, T., Speier, P.: Mr image reconstruction by using the iterative refinement method and nonlinear inverse scale space methods. *UCLA CAM Report*, pp. 06–35 (2006)
11. L1-magic: <http://www.acm.caltech.edu/l1magic>
12. Lustig, M., Donoho, D., Santos, J., Pauly, J.: Compressed sensing mri. *IEEE Sig. Proc. Magazine* (2007)
13. Ma, S., Yin, W., Zhang, Y., Chakraborty, A.: An efficient algorithm for compressed mr imaging using total variation and wavelets. *CVPR* (2008)
14. Maleh, R., Gilbert, A.C., Strauss, M.J.: Sparse gradient image reconstruction done faster. *ICIP* 2, 77–80 (2007)
15. Natarajan, B.K.: Sparse approximate solutions to linear systems. *SIAM Journal on Computing* 24, 227–234 (1995)
16. Romberg, J.: Variational methods for compressive sampling. *Proc. SPIE* 6498, 64980J–2–5 (2007)
17. Romberg, J.: Imaging via compressive sampling. *Comm. Pure Appl. Math.* 14–20 (2008)
18. Rudin, L., Osher, S., Fatemi, E.: Nonlinear total variation based noise removal algorithms. *Physica D Nonlinear Phenomena* 60(1), 259–268 (1992)
19. Saunders, M.A.: Pdco: Primal-dual interior-point method for convex objectives. *Systems Optimization Laboratory, Stanford University* (2002)
20. Skodras, A., Christopoulos, C., Ebrahimi, T.: The jpeg2000 still image compression standard. *IEEE Signal Processing Mag.* 18, 36–58 (2001)
21. SparseLab: <http://sparselab.stanford.edu>
22. Takhar, D., Laska, J., Wakin, M., Duarte, M., et al.: A new compressive imaging camera architecture using optical-domain compression. *Proc. of Computational Imaging IV at SPIE Electronic Imaging* 6065, 43–52 (2006)
23. Tropp, J.A., Gilbert, A.C.: Signal recovery from partial information via orthogonal matching pursuit. *IEEE Transactions on Information Theory* 53, 4655–4666 (2007)
24. Yang, J., Zhang, Y., Yin, W.: A fast tv-l1-l2 algorithm for image reconstruction from partial fourier data. To be submitted to *IEEE Trans. on Special Topics* (2008)